Progress In Electromagnetics Research B, Vol. 60, 95–110, 2014

Analytical Derivation of Induction Motors Inductances under Eccentricity Conditions

Hossein Hooshmandi,[1, *] Mohammad Ebrahimi[1, 2], Ali Davoudi[2], and Alireza Pouramin[1]

Abstract—Geometrical modeling of induction machines under eccentricity conditions involves a significant number of self and mutual inductances. These inductances are functions of rotor angular position, and calculating them at each time step requires solving computationally-intensive definite integrals. Conventional techniques use numerical look-up tables, or employ approximated analytical expressions such as limited-term Fourier series expression of turn functions. The former approach needs large memory volume given the size of inductance matrix. Moreover, numerical interpolations are needed upon model execution, which significantly slows down the simulation. The later technique is computationally tasking for a large set of Fourier series terms, or lacks sufficient accuracy if only a few terms are used. Alternatively, computationally efficient closed-form solutions for self- and mutual-inductance expressions are presented here. The step variations of turn functions are considered which streamlines the model formulation. The experimental results validate the proposed model. In particular, the frequency spectrum of the stator current illustrates the ability of proposed technique to detect eccentricity.

1. INTRODUCTION

Fault detection and diagnosis in induction motors is of paramount value, given the economy of scale, and the cost and time involved in the production halt and maintenance process. Mechanical faults amount to roughly 50–60% of all faults, and the air-gap eccentricity constitutes 80% of the mechanical fault [1, 2]. Air-gap eccentricity can be inherent due to the manufacturing imperfection, or appear over time by mechanical wear or unbalanced loads. The non-uniformity in the air-gap modifies machine inductances and flux paths, leading to the appearance of harmonic components in the stator current. Thus, the presence of harmonics in stator current spectrum can be used for eccentricity detection.

Numerical simulation of induction motors is essential to minimize hardware redesign and retrofit. The model should account for inductance variations due to the changing air-gap length; i.e., the current harmonics should appear in stator currents spectrum. First principle models, e.g., finite element methods (FEM), are highly accurate but computationally expensive [3–6]. Geometrical models, e.g., winding function methods (WFM) or mutual coupled circuit model (MCCM), are prevalent in the literature [7–11].

Existing studies calculate the inductance considering the space harmonics of the stator winding and rotor bars. WFM is used to analyze the transient behavior of IM under internal turn faults [10]. Saturation effects are included by modifying the air-gap length [11]. WFM models the IM under air-gap eccentricity faults in [12]. However, conventional WFM is not accurate with non-uniform air-gap in eccentricity conditions.

Received 17 May 2014, Accepted 7 June 2014, Scheduled 15 June 2014

* Corresponding author: Hossein Hooshmandi (h.hoshmandisafa@ec.iut.ac.ir).

[1] Department of Electrical and Computer Engineering, Isfahan University of Technology, Isfahan, Iran. [2] Department of Electrical Engineering, University of Texas at Arlington, USA.

An alternative approach, modified winding function (MWF), is presented to analyze IM performance under eccentricity conditions [13, 14]. In [15], a linear function is considered for magneto motive forces (MMF) variation in slot, and then stator-winding and eccentricity faults are analyzed [16, 17]. IM performance under inclined static eccentricity is studied in [18]. The fluctuation in stator inductance is used as an eccentricity index in [19]. MWF is used to find the mutual, self, and leakage inductances for a single-sided linear IM in [20].

Under eccentricity conditions, the variable air-gap leads to inductances that are functions of stator circumferential angle and rotor angular position. Thus, MWF needs to calculate all inductances at each time step. This is very time consuming given the large number of inductances considered and definite integrals involved in model formulation. As an example, an IM with 36 stator slots and 48 rotor bars requires calculating a total of 1378 self and mutual inductances for the stator and rotor at each time step.

One can save an inductance value as a numerical function of rotor angular positions in look-up tables for future use [21, 22]. The memory requirement can be tasking given large inductance matrices and required resolution on rotor's movement path. In [7] by a specific definition for the inverse air gap function, in the eccentric machine, indefinite integrals are determined and inductances are obtained. An alternative approach includes Fourier series representation of the stator and the rotor turn-functions [18, 23]; e.g., up to 10th harmonics are considered for a synchronous machine in [14]. Hybrid approaches, which include both Lookup tables and Fourier series of turn functions, are used in [16]. To properly capture the eccentricity effects in frequency spectrum of stator currents would require a large number of Fourier series terms, which makes the final model computationally prohibitive.

The objective of this paper is to analytically derive machine inductances under eccentricity conditions using the MFW method. To do this, the step variations of the turn functions are considered. The air-gap expression is adopted from [28, 29], and the inverse of air-gap function is considered, which streamlines the model formulation process. Moreover, a comprehensive step-by-step procedure is presented to develop self and mutual inductances for both stator and rotor. The model formulation is general, not limited to a fixed number of pole-pairs or stator slots, and applicable to variety of machine types. The proposed process is systematic and, hence, automatable.

This paper is organized as follows. Different eccentricity types are presented in Section 2. MWF is discussed in Section 3. In Section 4, IM inductances are calculated under different eccentricity conditions. In Section 5 transient model of IM under eccentricity condition is presented. Section 6 shows the capability of the proposed method in reflecting the eccentricity in stator current spectrum using both the numerical simulation and hardware experiments.

2. ECCENTRICITY TYPES AND THE AIR-GAP LENGTH

In healthy mode of operation, symmetrical axis of the rotor, symmetrical axis of the stator, and rotor rotation axis coincide and the air-gap is uniform. Under eccentricity conditions, aforementioned axes are displaced relative to each other, and the air-gap length varies with the rotor rotation and is a function of time. Figure 1 illustrates three forms of eccentricity: static eccentricity (SE), dynamic eccentricity (DE), and mixed eccentricity (ME) [24–27]. In SE, rotor symmetrical axis is coincide with its rotation axis, but is shifted from the stator symmetrical axis (Figure 1(a)). The minimum air-gap length is constant. In DE, the symmetrical axis of the stator coincides with the rotation axis of rotor, but both are shifted with respect to the rotor symmetrical axis (Figure 1(b)). The minimum air-gap length, therefore, varies as a function of rotor position. In ME, both static and dynamic eccentricities exist simultaneously (Figure 1(c)).

In general eccentricity condition, the air-gap function is given by [28, 29]:

$$g(\varphi, \theta_r) = g_0 \left(1 - e_s \cos(\varphi) - e_d \cos(\varphi - \theta_r)\right) \tag{1}$$

where φ is the stator circumferential angle, θ_r the rotor angle in mechanical degree, g_0 the length of the air-gap in symmetrical condition, and e_s and e_d are static and dynamic eccentricity coefficients.

The inverse of the air-gap length is needed to calculate machine inductances. This inverse can be approximated as [30]:

$$g^{-1}(\varphi, \theta_r) = G_0 + G_1 \cos(\varphi - \alpha) + G_2 \cos(2(\varphi - \alpha)) \tag{2}$$

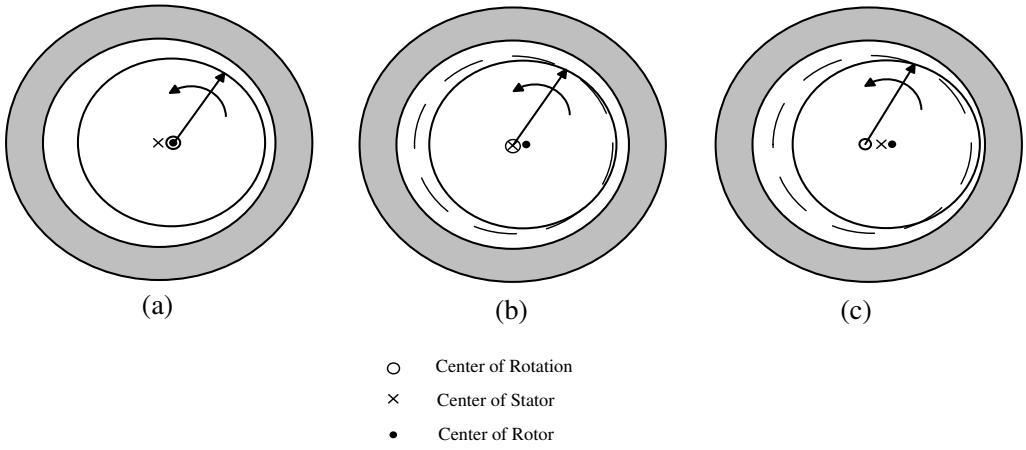

Figure 1. (a) Static, (b) dynamic, and (c) mixed eccentricity.

where coefficients $G_0,\ G_1,\ G_2$ and α are given by

$$G_0 = \frac{1}{g_0\sqrt{1-e^2}} \tag{3}$$

$$G_1 = \frac{2}{g_0\sqrt{1-e^2}}\left(\frac{1-\sqrt{1-e^2}}{e}\right) \tag{4}$$

$$G_2 = \frac{2}{g_0\sqrt{1-e^2}}\left(\frac{1-\sqrt{1-e^2}}{e}\right)^2 \tag{5}$$

$$\alpha = \tan^{-1}\left(\frac{e_d\sin\theta_r}{e_s+e_d\cos\theta_r}\right) \tag{6}$$

Coefficient e is the eccentricity coefficient

$$e = \sqrt{e_s^2+e_d^2+2e_se_d\cos\theta_r} \tag{7}$$

3. MODIFIED WINDING FUNCTIONS AND INDUCTANCE CALCULATION

The so-called modified winding function method [14] accounts for the air-gap eccentricity. The modified winding function of a coil, $M(\varphi,\theta_r)$, can be expressed as [8]

$$M(\varphi,\theta_r) = n(\varphi,\theta_r) - \langle M(\theta_r)\rangle \tag{8}$$

where $n(\varphi,\theta_r)$ is the turn function. $\langle M(\theta_r)\rangle$ is the average-value of the modified winding function given by [15]

$$\langle M(\theta_r)\rangle = \frac{1}{2\pi\left\langle g^{-1}(\varphi,\theta_r)\right\rangle}\int_0^{2\pi} n(\varphi,\theta_r)g^{-1}(\varphi,\theta_r)d\varphi \tag{9}$$

$$\left\langle g^{-1}(\varphi,\theta_r)\right\rangle = \frac{1}{2\pi}\int_0^{2\pi} g^{-1}(\varphi,\theta_r)d\varphi = G_0 \tag{10}$$

$$\langle M(\theta_r)\rangle = \frac{1}{2\pi G_0}\int_0^{2\pi} n(\varphi,\theta_r)g^{-1}(\varphi,\theta_r)d\varphi \tag{11}$$

One may re-write (11) to find the inductance

$$\int_0^{2\pi} n(\varphi,\theta_r)g^{-1}(\varphi,\theta_r)d\varphi = 2\pi G_0 \left\langle M(\theta_r)\right\rangle \tag{12}$$

The mutual inductance of coil A due to current presence in coil B can be found using the modified turn function and the inverse of air-gap as in [16]

$$L_{AB}(\theta_r) = \mu_0 r\ell \int_0^{2\pi} n_A(\varphi)M_B(\varphi,\theta_r)g^{-1}(\varphi,\theta_r)d\varphi \tag{13}$$

where μ_0 is the permeability of air, r the average radius of the air gap, and ℓ the stator's length. Substituting (8) in (13) provides

$$L_{AB}(\theta_r) = \mu_0 r\ell \left(\int_0^{2\pi} n_A(\varphi)n_B(\varphi)g^{-1}(\varphi,\theta_r)d\varphi - \int_0^{2\pi} \left\langle M_B(\theta_r)\right\rangle n_A(\varphi)g^{-1}(\varphi,\theta_r)d\varphi \right) \tag{14}$$

Since $\langle M_B(\theta_r)\rangle$ does not depend on φ, it can be brought out of the integral in (14)

$$L_{AB}(\theta_r) = \mu_0 r\ell \left(\int_0^{2\pi} n_A(\varphi)n_B(\varphi)g^{-1}(\varphi,\theta_r)d\varphi - \left\langle M_B(\theta_r)\right\rangle \int_0^{2\pi} n_A(\varphi)g^{-1}(\varphi,\theta_r)d\varphi \right) \tag{15}$$

Using (15), self and mutual inductances can be calculated under eccentricity condition. However, the average of modified winding functions for phase a, b and c is still needed (Equations (9)–(11)).

In the case of uniform air-gap, average of the turn function $\langle n(\theta_r)\rangle$ is constant. Under eccentricity conditions, $\langle n(\theta_r)\rangle$ depends on the rotor position. In this condition, $\langle n(\theta_r)\rangle$ is represented by$\langle M(\theta_r)\rangle$. Thus, $\langle M(\theta_r)\rangle$ should be found analytically, and its variation with the rotor position under different eccentricity conditions examined.

4. INDUCTANCE CALCULATION CONSIDERING ECCENTRICITY CONDITION

4.1. Representing the Turn Functions

The step variation form of the turn function of a concentrated winding is considered. The turn function of stator phase a, $n_a(\varphi)$, can be written as a step variation:

$$n_a(\varphi) = N\left[\sum_{i=0}^{\frac{N_S}{mP}-1} u\left(\varphi - i\frac{2\pi}{N_S}\right) - \sum_{i=\frac{3N_S}{mP}}^{\frac{4N_S}{mP}-1} u\left(\varphi - i\frac{2\pi}{N_S}\right) + \sum_{i=0}^{\frac{N_S}{mP}-1} u\left(\varphi - i\frac{2\pi}{N_S} - \pi\right) - \sum_{i=\frac{3N_S}{mP}}^{\frac{4N_S}{mP}-1} u\left(\varphi - i\frac{2\pi}{N_S} - \pi\right)\right] \tag{16}$$

where $u(\varphi)$ represents an step function. m, P, and N_S are number of stator phases, number of pole pairs, and slot numbers, respectively. Turn functions for stator phases b and c can be readily obtained by phase shifting

$$n_b(\varphi) = n_a\left(\varphi - \frac{4\pi}{mP}\right) \tag{17}$$

$$n_c(\varphi) = n_a\left(\varphi - \frac{8\pi}{mP}\right) \tag{18}$$

A motor with 4 poles, 36 stator slots, and 48 rotor bars is considered in this paper. Figure 2 shows the turn function for stator phase a. This turn function and associated MWF can be expressed as a combination of step functions

$$n_a(\varphi) = N\left(\sum_{k=0,1,2,18,19,20} u\left(\varphi - k\frac{\pi}{18}\right) - \sum_{k=9,10,11,27,28,29} u\left(\varphi - k\frac{\pi}{18}\right)\right) \tag{19}$$

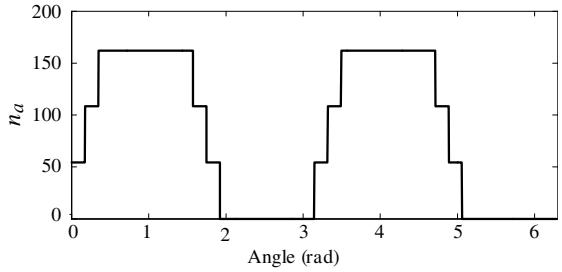

Figure 2. Turns function $n_a(\varphi)$ of stator phase a.

4.2. Average of Modified Winding Function

Average-value of the modified winding function for the stator phase a is given by (11) and written here for convenience

$$\langle M_a(\theta_r)\rangle = \frac{1}{2\pi G_0}\int_0^{2\pi} n_a(\varphi)g^{-1}(\varphi,\theta_r)d\varphi \tag{20}$$

Substituting the inverse air-gap function (2) in (20) gives

$$\langle M_a(\theta_r)\rangle = \frac{1}{2\pi G_0}\left(3N\pi G_0 - NG_1\left(\begin{array}{l}\displaystyle\sum_{i=0}^{\frac{N_S}{2mP}-1}\sin\left(i\frac{2\pi}{N_S}-\alpha\right)\\ \displaystyle+\sum_{i=\frac{3N_S}{2mP}}^{\frac{2N_S}{mP}-1}\sin\left(i\frac{2\pi}{N_S}-\alpha\right)\end{array}\right) - \frac{NG_2}{2}\left(\begin{array}{l}\displaystyle\sum_{i=0}^{\frac{N_S}{2mP}-1}\sin\left(i\frac{2\pi}{N_S}-\alpha\right)+\\ \displaystyle\sum_{i=\frac{3N_S}{2mP}}^{\frac{2N_S}{mP}-1}\sin\left(i\frac{2\pi}{N_S}-\alpha\right)-\frac{NG_2}{2}\end{array}\right)\right) \tag{21}$$

Here, N is the number of series-connected turns in the stator coil. G_1, G_2 and α depend on the rotor position. Average-value of the modified winding function for the stator phase b and c can be found by phase shifting:

$$\langle M_b(\theta_r)\rangle = M_a\left(\theta_r - \frac{4\pi}{mP}\right) \tag{22}$$

$$\langle M_c(\theta_r)\rangle = M_a\left(\theta_r - \frac{8\pi}{mP}\right) \tag{23}$$

For the motor example in this paper, with the phase-a turn function given in (19), the average-value of modified turn function is given in (24)

$$\begin{aligned}\langle M_a(\theta_r)\rangle = \frac{1}{2\pi G_0}&\left(3N\pi G_0 + NG_1\left(\begin{array}{l}\displaystyle\sum_{k=0,1,2,18,19,20}\sin\left(\alpha - k\frac{\pi}{18}\right) -\\ \displaystyle\sum_{k=9,10,11,27,28,29}\sin\left(\alpha - k\frac{\pi}{18}\right)\end{array}\right)\right.\\ &\left.+\frac{NG_2}{2}\left(\begin{array}{l}\displaystyle\sum_{k=0,1,2,18,19,20}\sin 2\left(\alpha - k\frac{\pi}{18}\right)\\ \displaystyle-\sum_{k=9,10,11,27,28,29}\sin 2\left(\alpha - k\frac{\pi}{18}\right)\end{array}\right)\right)\end{aligned} \tag{24}$$

Similarly, $\langle M_b(\theta_r)\rangle$ and $\langle M_c(\theta_r)\rangle$ can be extracted. Using (15) and (24), the inductance values can be calculated.

4.3. Stator Inductance

4.3.1. Self Inductance of Stator Phase a

Using (15), the self-inductance of stator phase a is

$$L_{s(aa)}(\theta_r) = \mu_0 r\ell \left(\int_0^{2\pi} n_a(\varphi) n_a(\varphi) g^{-1}(\varphi, \theta_r) d\varphi - \langle M_a(\theta_r) \rangle \int_0^{2\pi} n_a(\varphi) g^{-1}(\varphi, \theta_r) d\varphi \right) \tag{25}$$

The first term can be defined as

$$I_a = \int_0^{2\pi} n_a(\varphi) n_a(\varphi) g^{-1}(\varphi, \theta_r) d\varphi \tag{26}$$

It should be noted that I_a is calculated similar to $\langle M_a(\theta_r) \rangle$.

$$\begin{aligned}
I_a &= \int_0^{2\pi} n_a(\varphi) n_a(\varphi) g^{-1}(\varphi, \theta_r) d\varphi \\
&= \frac{146 N^2 \pi G_0}{18} + G_1 N^2 \left(\sin\alpha - 3\sin\left(\frac{\pi}{18} - \alpha\right) - 5\sin\left(\frac{\pi}{9} - \alpha\right) + 5\sin\left(\frac{\pi}{2} - \alpha\right) \right. \\
&\quad + 3\sin\left(\frac{10\pi}{18} - \alpha\right) + \sin\left(\frac{11\pi}{18} - \alpha\right) - \sin(\pi - \alpha) - 3\sin\left(\frac{19\pi}{18} - \alpha\right) - 5\sin\left(\frac{20\pi}{18} - \alpha\right) \\
&\quad \left. + 5\sin\left(\frac{3\pi}{2} - \alpha\right) + 3\sin\left(\frac{28\pi}{18} - \alpha\right) + \sin\left(\frac{29\pi}{18} - \alpha\right) \right) \\
&\quad + \frac{G_2 N^2}{2} \left(\sin 2\alpha - 3\sin 2\left(\frac{\pi}{18} - \alpha\right) - 5\sin 2\left(\frac{\pi}{9} - \alpha\right) + 5\sin 2\left(\frac{\pi}{2} - \alpha\right) + 3\sin 2\left(\frac{10\pi}{18} - \alpha\right) \right. \\
&\quad + \sin 2\left(\frac{11\pi}{18} - \alpha\right) - \sin 2(\pi - \alpha) - 3\sin 2\left(\frac{19\pi}{18} - \alpha\right) - 5\sin 2\left(\frac{20\pi}{18} - \alpha\right) \\
&\quad \left. + 5\sin 2\left(\frac{3\pi}{2} - \alpha\right) + 3\sin 2\left(\frac{28\pi}{18} - \alpha\right) + \sin 2\left(\frac{29\pi}{18} - \alpha\right) \right)
\end{aligned} \tag{27}$$

Substituting (12) and (26) in (25), the self-inductance of phase a is

$$L_{s(aa)}(\theta_r) = \mu_0 r\ell \left(I_a - 2\pi G_0 \left(\langle M_a(\theta_r) \rangle \right)^2 \right) \tag{28}$$

With substitution of $\langle M_a(\theta_r) \rangle$ from (24) and I_a from (27) in (28), the self inductance of stator phase a is found analytically. L_{bb} and L_{cc} can also be calculated similarly. Figure 3 illustrates the self-inductance of the stator phase a under different eccentricity conditions, for the motor parameters summarized in the appendix.

4.3.2. Mutual Inductance between Stator Phases

Using (15), the mutual inductance between phases a and b of the stator can be written as:

$$L_{s(ab)}(\theta_r) = \mu_0 r\ell \left(\int_0^{2\pi} n_a(\varphi) n_b(\varphi) g^{-1}(\varphi, \theta_r) d\varphi - \langle M_b(\theta_r) \rangle \int_0^{2\pi} n_a(\varphi) g^{-1}(\varphi, \theta_r) d\varphi \right) \tag{29}$$

$$L_{s(ab)}(\theta_r) = \mu_0 r\ell \left(I_{ab} - 2\pi G_0 \langle M_a(\theta_r) \rangle \langle M_b(\theta_r) \rangle \right) \tag{30}$$

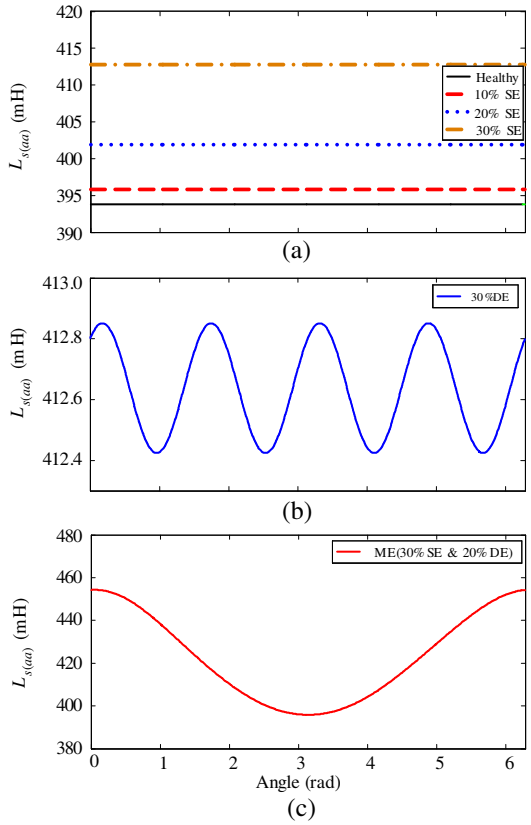

Figure 3. Self inductance of stator phase a: (a) healthy and different SE condition, (b) 30% DE, and (c) ME (30% SE and 20% DE).

where, I_{ab} is found using the turn functions of phases a and b

$$I_{ab} = 3N^2\pi G_0 + 3G_1N^2\left(\sum_{k=6,7,8,24,25,26}\sin\left(\alpha - k\frac{\pi}{18}\right) - \sum_{k=9,10,11,27,28,29}\sin\left(\alpha - k\frac{\pi}{18}\right)\right)$$
$$+\frac{3G_2N^2}{2}\left(\sum_{k=6,7,8,24,25,26}\sin 2\left(\alpha - k\frac{\pi}{18}\right) - \sum_{k=9,10,11,27,28,29}\sin 2\left(\alpha - k\frac{\pi}{18}\right)\right) \quad (31)$$

According to (15), this equation is commutative. Therefore

$$L_{s(ba)}(\theta_r) = L_{s(ab)}(\theta_r) \quad (32)$$

Mutual inductance of other phases can be found similarly. Figure 4 illustrates the mutual inductance between stator phases a and b in the healthy mode of operation as well as different SE conditions. Figures 5 and 6 illustrate the mutual inductance between stator phase a and b in 30% DE and different ME conditions, respectively.

4.4. Rotor Inductance

Using (15), the inductance term between rotor loops i and j can be expressed as

$$L_{r(ij)}(\theta_r) = \mu_0 r\ell\left(\int_0^{2\pi} n_i(\varphi,\theta_r)n_j(\varphi,\theta_r)g^{-1}d\varphi - \langle M_j(\theta_r)\rangle\int_0^{2\pi} n_i(\varphi,\theta_r)g^{-1}d\varphi\right) \quad (33)$$

where, $n_i(\varphi,\theta_r)$ and $n_j(\varphi,\theta_r)$ are turn functions of rotor loops i and j, respectively:

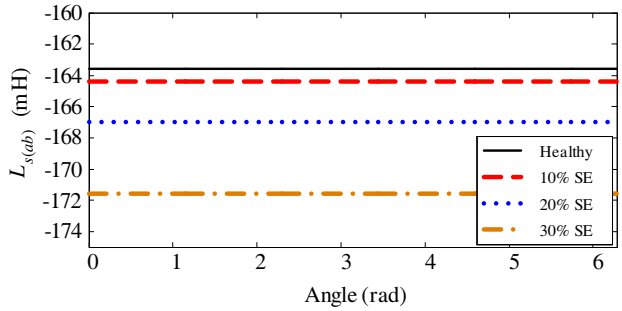

Figure 4. Mutual inductance between stator phases a and b in the healthy mode of operation as well as different SE conditions.

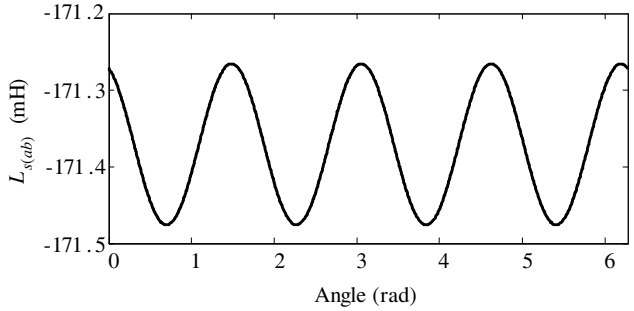

Figure 5. Mutual inductance between stator phases a and b in 30% DE.

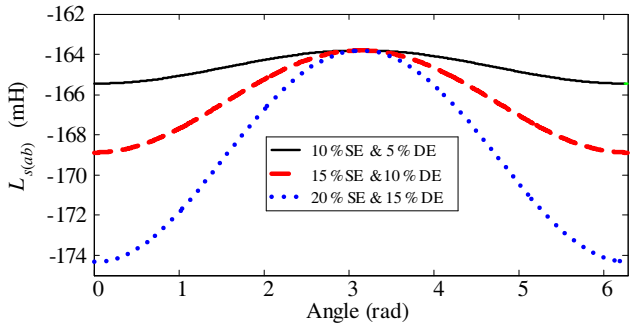

Figure 6. Mutual inductance between stator phases a and b under different ME conditions.

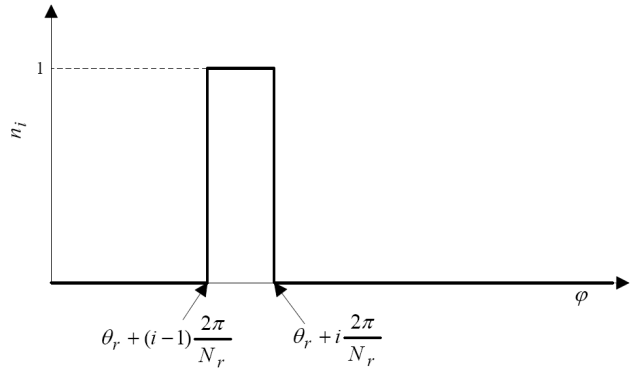

Figure 7. Turn function of a rotor loop.

Figure 7 illustrates turn function of a rotor loop that is one only in $\theta_r + (i-1)\frac{2\pi}{N_r} \leq \varphi \leq \theta_r + i\frac{2\pi}{N_r}$ interval and is zero elsewhere.

If $i = j$, by setting the rotor turn function value in (33) to 1, (33) is simplified as:

$$L_{r(ii)}(\theta_r) = \mu_0 r \ell \left(\int_{\theta_r+(i-1)\frac{2\pi}{N_r}}^{\theta_r+i\frac{2\pi}{N_r}} g^{-1}(\varphi, \theta_r) d\varphi - \langle M_i(\theta_r) \rangle \int_{\theta_r+(i-1)\frac{2\pi}{N_r}}^{\theta_r+i\frac{2\pi}{N_r}} g^{-1}(\varphi, \theta_r) d\varphi \right) \tag{34}$$

Using (11), the average-value of the modified winding function of the rotor loop i is given by:

$$\langle M_i(\theta_r) \rangle = \frac{1}{2\pi G_0} \int_{\theta_r+(i-1)\frac{2\pi}{N_r}}^{\theta_r+i\frac{2\pi}{N_r}} g^{-1}(\varphi, \theta_r) d\varphi \tag{35}$$

Or

$$\int_{\theta_r+(i-1)\frac{2\pi}{N_r}}^{\theta_r+i\frac{2\pi}{N_r}} g^{-1}(\varphi, \theta_r) d\varphi = 2\pi G_0 \langle M_i(\theta_r) \rangle \tag{36}$$

inserting (36) in (34) will result in

$$L_{r(ii)}(\theta_r) = \mu_0 r \ell \left(2\pi G_0 \langle M_i(\theta_r) \rangle - 2\pi G_0 \left(\langle M_i(\theta_r) \rangle \right)^2 \right) \tag{37}$$

If $i \neq j$, the two loops of i and j do not have any common points, and the first term in (33) will be zero:

$$L_{r(ij)}(\theta_r) = -\mu_0 r\ell \left(2\pi G_0\right) \langle M_i(\theta_r)\rangle \langle M_j(\theta_r)\rangle \tag{38}$$

The average-value of the modified winding function is needed to find the rotor loop inductance. First, l and h are defined as

$$l = \theta_r + (i-1)\frac{2\pi}{N_r} \tag{39}$$

$$h = \theta_r + i\frac{2\pi}{N_r} \tag{40}$$

$$\begin{aligned}\langle M_i(\theta_r)\rangle &= \frac{1}{2\pi G_0} \int\limits_{\theta_r+(i-1)\frac{2\pi}{N_r}}^{\theta_r+i\frac{2\pi}{N_r}} g^{-1}(\varphi,\theta_r)d\varphi = \frac{1}{2\pi G_0}\int\limits_{l}^{h} g^{-1}(\varphi,\theta_r)d\varphi \\ &= \frac{1}{2\pi G_0}\left(\frac{2\pi G_0}{N_r} + G_1\left(\sin(h-\alpha)-\sin(l-\alpha)\right) + \frac{G_2}{2}\left(\sin 2(h-\alpha)-\sin 2(l-\alpha)\right)\right)\end{aligned} \tag{41}$$

The average-value of the modified winding function is calculated for any rotor loop from (41). By replacing this value in (37) and (38), self and mutual inductances of rotor loops can be found. Figures 8 and 9 show the self-inductance of rotor loop 1 and mutual inductance between the rotor loops 1 and 2 in different eccentricity conditions, respectively.

4.5. Mutual Inductance between the Stator Phases and Rotor Loops

Using (15), the mutual inductance between stator phase a and rotor loop i is given by:

$$L_{sr(ai)}(\theta_r) = \mu_0 r\ell \left(\int\limits_0^{2\pi} n_a(\varphi)n_i(\varphi)g^{-1}(\varphi,\theta_r)d\varphi - \langle M_i(\theta_r)\rangle \int\limits_0^{2\pi} n_a(\varphi)g^{-1}(\varphi,\theta_r)d\varphi\right) \tag{42}$$

The first term of (42) can be written as:

$$I_{ai} = \int\limits_0^{2\pi} n_a(\varphi)n_i(\varphi)g^{-1}(\varphi,\theta_r)d\varphi \tag{43}$$

The second term of (33) is expressed as

$$\int\limits_0^{2\pi} n_a(\varphi)g^{-1}(\varphi,\theta_r)d\varphi = 2\pi G_0 \langle M_a(\theta_r)\rangle \tag{44}$$

Thus, (42) can be simplified to

$$L_{sr(ai)}(\theta_r) = \mu_0 r l \left(I_{ai} - 2\pi G_0 \langle M_a(\theta_r)\rangle \langle M_i(\theta_r)\rangle\right) \tag{45}$$

In (45), $\langle M_a(\theta_r)\rangle$ and $\langle M_i(\theta_r)\rangle$ are already found. Thus, it is only necessary to calculate I_{ai}. Since the turn function of the ith rotor loop, $n_i(\varphi)$, is 1 only in $\theta_r + (i-1)\frac{2\pi}{N_r} \leq \varphi \leq \theta_r + i\frac{2\pi}{N_r}$ interval and is zero elsewhere,

$$I_{ai} = \int\limits_0^{2\pi} n_a(\varphi)n_i(\varphi)g^{-1}(\varphi,\theta_r)d\varphi = \int\limits_{\theta_r+(i-1)\frac{2\pi}{N_r}}^{\theta_r+i\frac{2\pi}{N_r}} n_a(\varphi)g^{-1}(\varphi,\theta_r)d\varphi = \int\limits_{l}^{h} n_a(\varphi)g^{-1}(\varphi,\theta_r)d\varphi \tag{46}$$

Since $n_a(\varphi)$ is the sum of step variations, to find I_{ai}, first an integral must be calculated for a sample step function:

$$\begin{aligned} I &= \int_{l}^{h} u\left(\varphi-\varphi_0\right) g^{-1}(\varphi,\theta_r)d\varphi \\ &= G_0\left(h-\varphi_0\right)u(h-\varphi_0)+G_1 u\left(h-\varphi_0\right)\left(\sin\left(h-\alpha\right)+\sin(\alpha-\varphi_0)\right) \\ &\quad +\frac{G_2}{2}u\left(h-\varphi_0\right)\left(\sin 2\left(h-\alpha\right)+\sin 2\left(\alpha-\varphi_0\right)\right)-G_0\left(l-\varphi_0\right)u(l-\varphi_0) \\ &\quad -G_1 u\left(l-\varphi_0\right)\left(\sin\left(l-\alpha\right)+\sin(\alpha-\varphi_0)\right)-\frac{G_2}{2}u\left(l-\varphi_0\right)\left(\sin 2\left(l-\alpha\right)+\sin 2\left(\alpha-\varphi_0\right)\right) \end{aligned} \quad (47)$$

The turn function, φ_0, can be written as the coefficients of $\frac{\pi}{18}$:

$$\varphi_{0ja}=k_{ja}\frac{\pi}{18} \qquad j=1,2\ldots,12 \quad (48)$$

where j is the number of steps in the turn function of stator phases. For stator phase a, k_j is given by

$$k_{ja}=0,1,2,9,10,11,18,19,20,27,28,29 \qquad j=1,2\ldots,12 \quad (49)$$

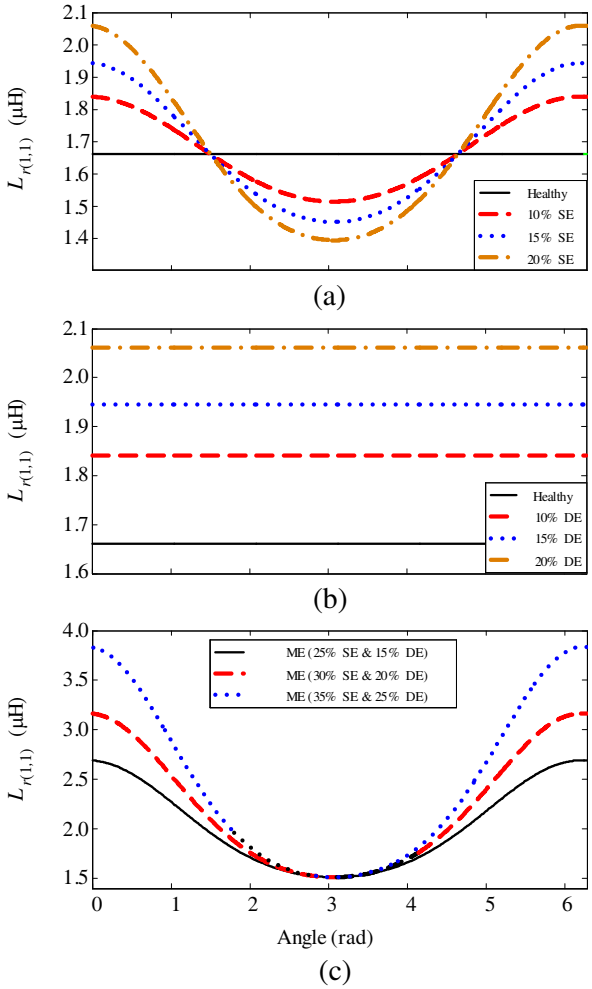

Figure 8. Self inductance of the rotor loop 1: (a) healthy and different SE condition, (b) healthy and different DE conditions, and (c) different ME conditions.

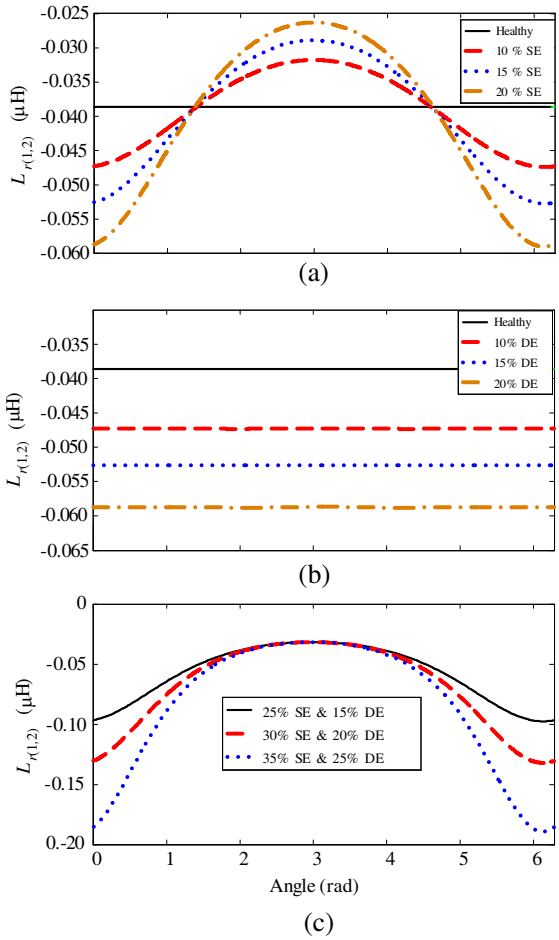

Figure 9. Mutual inductance between the rotor loop 1 and 2: (a) healthy and different SE conditions, (b) healthy and different DE conditions, and (c) different ME conditions.

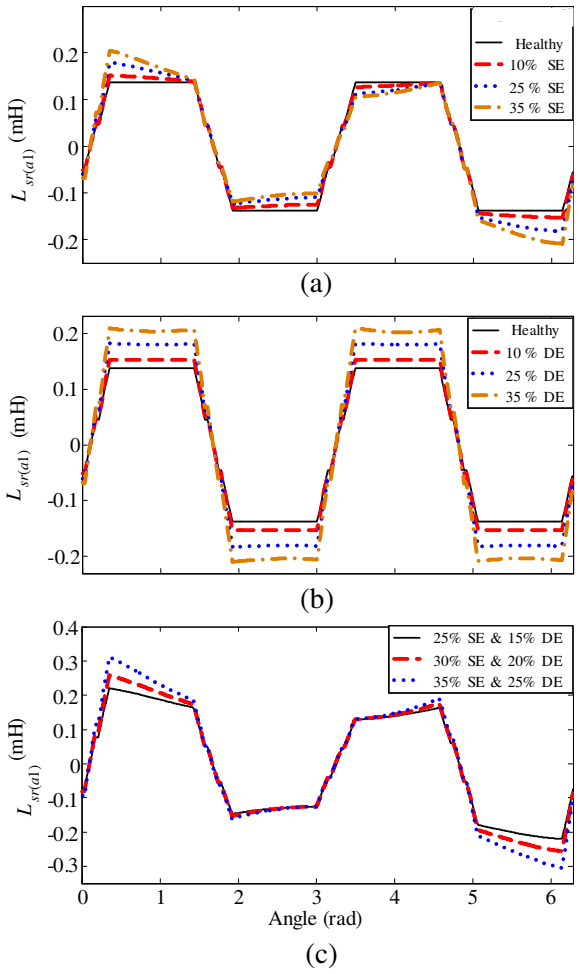

Figure 10. Mutual inductance between the stator phase a and rotor loop 1: (a) healthy and different SE condition, (b) healthy and different DE conditions, and (c) different ME conditions.

Using (47)–(49), I_{ai} will be obtained:

$$I_{ja} = I(\varphi = \varphi_{0ja}) \tag{50}$$

$$I_{ai}(\varphi, \theta_r) = N\left(\sum_{j=1,2,3,7,8,9} I_{ja} - \sum_{j=4,5,6,10,11,12} I_{ja}\right) \tag{51}$$

With substitution of $\langle M_a(\theta_r)\rangle$ from (25), $\langle M_i(\theta_r)\rangle$ from (41) and I_{ai} from (51) in (45), mutual inductance between stator phase and rotor loop can be found. Figure 10 illustrates the mutual inductance between the stator phase a and rotor loop 1 under different eccentricity conditions.

5. TRANSIENT MODEL OF AN INDUCTION MOTOR UNDER ECCENTRICITY CONDITION

General dynamic equations of induction motor are given by [12]

$$\mathbf{V_s} = \mathbf{R_s I_s} + \mathbf{L_{ss}}\frac{d\mathbf{I_s}}{dt} + \mathbf{L_{sr}}\frac{d\mathbf{I}_r}{dt} + \omega_r \frac{d\mathbf{L_{sr}}}{d\theta_r}\mathbf{I_r} \tag{52}$$

$$\mathbf{V_r} = \mathbf{R_r I_r} + \mathbf{L_{rr}}\frac{d\mathbf{I_r}}{dt} + \mathbf{L_{rs}}\frac{d\mathbf{I_s}}{dt} + \omega_r \frac{d\mathbf{L_{rs}}}{d\theta_r}\mathbf{I_s} \tag{53}$$

$$\omega_r = \frac{d\theta_r}{dt} \tag{54}$$

$$T_e - T_L = J\frac{d\omega_r}{dt} \tag{55}$$

where $\mathbf{V}$, $\mathbf{I}$, $\mathbf{R}$ and $\mathbf{L}$ are vectors of voltage, current resistance, and inductance matrices, respectively. θ_r is the rotor position, ω_r the angular speed, J the inertia moment of the rotor, and T_e and T_L are the electromagnetic and load torques, respectively.

Electromagnetic torque is obtained from co-energy,

$$T_e = \frac{\partial W_{co}}{\partial \theta_r} \tag{56}$$

which, for a linear system, is equal to the energy stored in the air gap

$$W_{co} = \frac{1}{2}\left(\mathbf{I_s^T L_{ss} I_s} + \mathbf{I_s^T L_{sr} I_r} + \mathbf{I_r^T L_{rs} I_s} + \mathbf{I_r^T L_{rr} I_r}\right) \tag{57}$$

The $\mathbf{L_{ss}}$ is 3×3 matrix and is obtained from (28) and (30). $\mathbf{L_{rr}}$ is 49×49 matrix and is obtained from (37) and (38). $\mathbf{L_{sr}}$ is 3×49 matrix and is obtained from (45), and $\mathbf{L_{rs}} = (\mathbf{L_{sr}})^{\mathbf{T}}$.

6. CASE STUDIES

An experimental test was carried out on a 4-pole 380-V, 2.2 kW induction motor with 48 rotor bars and 0.42 mm air gap. The stator winding is Y-connected. To induce eccentricity conditions, the original sleeves and rotor shaft were replaced. To produce static eccentricity, the sleeves are shifted from the center point. To produce dynamic eccentricity, the rotor shaft has been shifted from the center. A combination of both modified sleeve and displaced rotor shaft were used to create mixed eccentricity coordination. Figure 11 shows different motor parts.

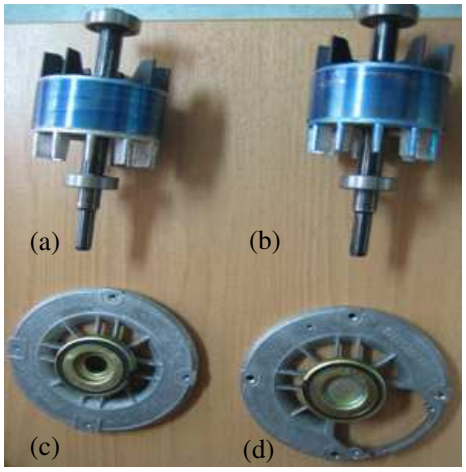

Figure 11. Experimental test rig: (a) healthy rotor, (b) rotor shaft has been shifted from the center, (c) and (d) sleeves have been shift from the center point.

The stator current spectrum is obtained by solving the dynamic model of the induction machine (52)–(57). The mixed eccentricity fault generates harmonic frequencies [6, 25]:

$$f_{ecc} = f_s(1 \pm k(1-s)/P) \quad k = 1, 2, 3, \ldots \tag{58}$$

where f_s is the supplied frequency, s the motor slip, and p the number of pair poles.

Figure 12 illustrates stator current under mixed eccentricity conditions (46% SE and 35% DE). Figure 12(a) shows stator current where only three terms of the Fourier series are used for the turn function in inductance formulation. Figures 12(b) and 12(c) show stator current predicted by the proposed method and experiments, respectively, which clearly show close resemblance.

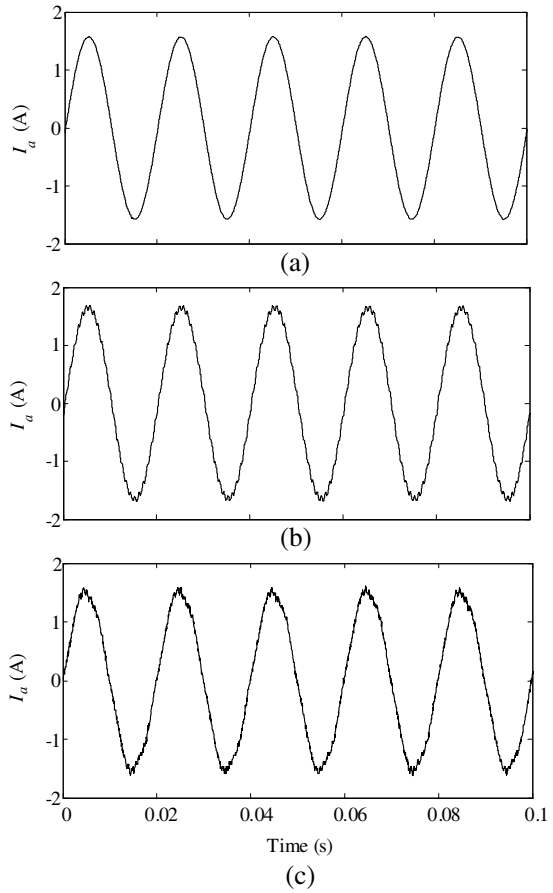

Figure 12. The stator current waveform in the steady-state under mixed eccentricity (46% SE and 35% DE: (a) using Fourier series of turn function, (b) using the proposed method, and (c) experimental results.

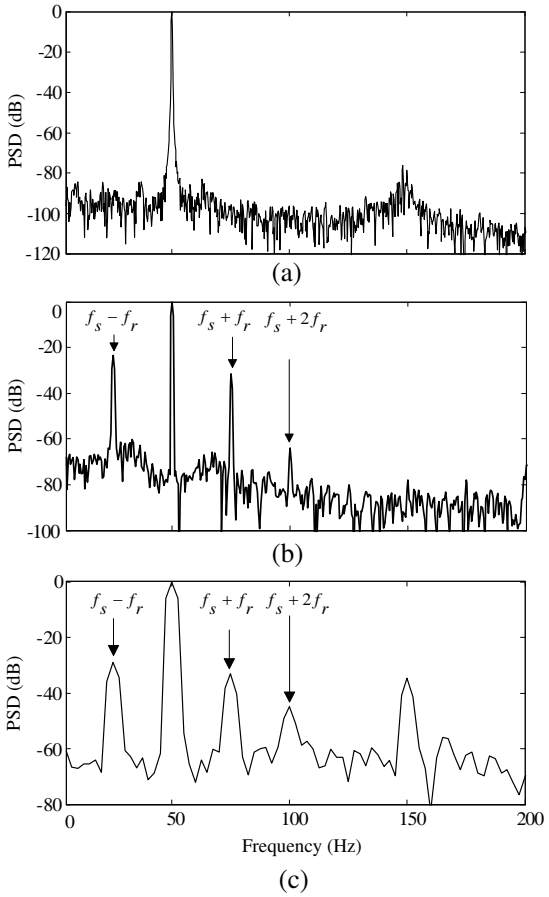

Figure 13. Normalized stator current spectra under mixed eccentricity (46% SE and 35% DE): (a) by using limited terms in the Fourier series of turn function, (b) by using the proposed method and, (c) experimentally.

Table 1. parameters of simulated motor.

Quantity	Value	Units
Rated power	2.2	kW
Rated voltage	380	V
Rated frequency	50	Hz
Number of poles	4	—
Number of stator slots	36	—
Number of rotor bars	48	—
Air gap length	0.42	mm

The line current is measured with the sampling frequency of 10 kHz. The amplitude of the sideband components around the fundamental harmonic can be extracted from the spectrum analysis of stator current for both healthy and faulty conditions. This will be used as an index for mixed-eccentricity fault detection. Figure 13 shows the power spectral density (PSD) of the line current in presence of mixed eccentricity. Figure 13(a) shows the normalized stator current spectra obtained by using the three terms of the Fourier series in formulating the turn function. Given the approximations involved

in describing turn functions, the harmonics related to eccentricity fault is not shown in the current spectra, and the eccentricity fault cannot be detected. On the other hand, as seen in Figure 13(b), the proposed approach successfully detects the harmonics related to the eccentricity faults. This is verified by the experimental results in Figure 13(c).

7. CONCLUSION

An analytical approach for inductance formulation of three-phase induction motors, under eccentricity condition, is presented. The inductance formulation includes infinite integrals of turn functions and calculation of this integral using numerical methods will be computationally intensive and time consuming. This paper considers the turn functions as a collection of step functions, which renders the analytical derivation of machine inductances practical. All inductances are obtained using trigonometric identities as functions of rotor position. The proposed model is significantly faster than those implemented via lookup tables and more accurate than those established using limited Fourier series terms. Experimental measurements and numerical simulation validate the effectiveness of the proposed methodology.

ACKNOWLEDGMENT

The authors would like to thank G. Esfandiari, S. Abhinav, and R. Sharifi, for helpful suggestions.

APPENDIX A. NOMENCLATURE

θ_r	Rotor angle (in mechanical degree)
φ	Rotor circumferential angle
ℓ	Stack length
r	Air gap average radius
N_s	Number of slot
m	number of phase
P	Number of pole
μ_0	Air permeability
g_0	Air-gap length in symmetrical condition
$g(\varphi, \theta_r)$	Air-gap length in nonsymmetrical condition
e_s	Static eccentricity coefficient
e_d	Dynamic eccentricity coefficient
e	Eccentricity coefficient
$n_i(\varphi, \theta_r)$	Turn function of winding i
$N_i(\varphi, \theta_r)$	Winding function of winding i
$M_i(\varphi, \theta_r)$	Modified winding function of winding i
$\langle n_i(\varphi, \theta_r)\rangle$	Average of turn function of winding i
$\langle M_i(\theta_r)\rangle$	Average of modified winding function of winding i

REFERENCES

1. Nandi, S., T. C. Ilamparithi, S. B. Lee, and D. Hyun, "Detection of eccentricity faults in induction machines based on nameplate parameters," *IEEE Trans. Ind. Elec.*, Vol. 58, No. 5, 1673–1683, May 2011.
2. Ilamparithi, T. C. and S. Nandi, "Detection of eccentricity faults in three-phase reluctance synchronous motor," *IEEE Trans. on Ind. Apps.*, Vol. 48, No. 4, 1307–1317, Jul.–Aug. 2012.

3. Hyun, D., J. Hong, S. B. Lee, K. Kim, E. J. Wiedenbrug, M. Teska, and S. Nandi, "Automated monitoring of airgap eccentricity for inverter-fed induction motors under standstill conditions," *IEEE Trans. Ind. Apps.* Vol. 47, No. 3, 1257–1266, May–Jun. 2011.
4. Ebrahimi, B. M. and J. faiz, "Configuration impacts on eccentricity fault detection in permanent magnet synchronous motors," *IEEE Trans. on Magnetics*, Vol. 48, No. 3, 903–906, Feb. 2012.
5. Torkaman, H., E. Afjei, and P. Yadegari, "Static, dynamic, and mixed eccentricity faults diagnosis in switched reluctance motors using transient finite element method and experiments," *IEEE Trans. on Magnetics*, Vol. 48, No. 3, 2254–2264, Aug. 2012.
6. Faiz, J., B. M. Ebrahimi, B. Akin, and H. A. Toliyat, "Comprehensive eccentricity fault diagnosis in induction motors using finite element method," *IEEE Trans. on Magnetics*, Vol. 45, No. 3, 1764–1767, Mar. 2009.
7. Faiz, J. and M. Ojaghi, "Unified winding function approach for dynamic simulation of different kinds of eccentricity faults in cage induction machines," *IET Elect. Power Appl.*, Vol. 3, 461–470, Sep. 2009.
8. Schmitz, N. L. and D. W. Novotny, *Introductory Electro. Mechanics*, Ch. 4, Roland Press, New York, 1965.
9. Toliyat, H. A. and T. A. Lipo, "Analysis of a concentrated winding induction machine for adjustable speed drive application. Part 1: Motor analysis," *IEEE Trans. Energy Conversion*, Vol. 6, No. 4, 679–684, Dec. 1991.
10. Toliyat, H. A. and M. M. Rahimian, "Transient analysis of cage induction machines under internal faults using winding function," *3rd Int. Conf. Electrical Rotating Machines — ELROMA*, 1992.
11. Moreria, J. C. and T. A. Lipo, "Modeling of saturated AC machines including air gap flux harmonic components," *IEEE Trans. Ind. Apps.*, Vol. 28, No. 2, 343–349, Mar.–Apr. 1992.
12. Toliyat, H. A., M. S. Arefeen, and G. Parlos, "A method for dynamic simulation of air-gap eccentricity in induction machines," *IEEE Trans. Ind. Apps.*, Vol. 32, No. 4, 910–918, Jul.–Aug. 1996.
13. Toliyat, H. A. and N. A. Al-Nuaim, "Simulation and detection of dynamic air-gap eccentricity in salient pole synchronous machines," *IEEE Ind. Apps. Society Annual Meeting*, Vol. 35, No. 1, 86–93, New Orleans, Louisiana, Oct. 1997.
14. Al-Nuaim, N. A. and H. A. Toliyat, "A novel method for modeling dynamic air-gap eccentricity in synchronous machines based on modified winding function theory," *IEEE Trans. Energy Conversion*, Vol. 13, No. 2, 156–162, Jun. 1998.
15. Joksimovic, M. G., D. M. Durovic, and A. B. Obradovic, "Skew and linear rise of MMF across slot modeling winding function approach," *IEEE Trans. Energy Conversion*, Vol. 14, 315–320, Sep. 1999.
16. Joksimovic, M. G., D. M. Durovic, J. Penman, and N. Arthur, "Dynamic simulation of dynamic eccentricity in induction machines-winding function approach," *IEEE Trans. Energy Conversion*, Vol. 15, No. 2, 143–148, Jun. 2000.
17. Joksimovic, M. G. and J. Penman, "The detection of inter-turn short circuits in the stator windings of operation motors," *IEEE Trans. Ind. Electronics*, Vol. 47, 1078–1084, Oct. 2000.
18. Li, X., Q. Wu, and S. Nandi, "Performance analysis of a three-phase induction machine with inclined static eccentricity," *IEEE Trans. Ind. Appl.*, Vol. 43, No. 2, Mar.–Apr. 2007.
19. Faiz, J. and M. Ojaghi "Stator inductance fluctuation of induction motor as an eccentricity fault index," *IEEE Trans. on Magnetics*, Vol. 47, No. 6, 531–541, 1775–1785, Jun. 2011.
20. Xu, W., G. Sun, G. Wen, Z. Wu, and P. K. Chu, "Equivalent circuit derivation and performance analysis of a single-sided linear induction motor based on the winding function theory," *IEEE Trans. Vehicular Technology*, Vol. 61, No. 4, 1515–11525, May 2012.
21. Luo, X., Y. Liao, H. A. Toliyat, A. El-Antably, and T. A. Lipo, "Multiple coupled circuit modeling of induction machines," *IEEE Trans. Ind. Appl.*, Vol. 31, No. 2, 311–318, Mar.–Apr. 1995.
22. Tabatabaei, I., J. faiz, H. Lesani, and M. T. Nabavi-Razavi, "Modeling and simulation of a salient-pole synchronous generator with dynamic eccentricity using modified winding function theory,"

IEEE Trans. on Magnetics, Vol. 40, No. 3, 1550–1555, May 2004.

23. Faiz, J., I. Tabatabaei, and E. Sharifi, "A precise electromagnetic modeling and performance analysis of a three-phase squirrel-cage induction motor under mixed eccentricity condition," *Electromagnetics*, 471–489, Jun. 2004.
24. Dorrell, D., "Sources and characteristics of unbalanced magnetic pull in three-phase cage induction motors with axial-varying rotor eccentricity," *IEEE Trans. Ind. Appl.,* Vol. 47, No. 1, Jan.–Feb. 2011.
25. Hyun, D., S. Lee, J. Hong, S. B. Lee, and S. Nandi, "Detection of airgap eccentricity for induction motors using the single-phase rotation test," *IEEE Trans. on Energy Conversion*, Vol. 27, No. 3, Sep. 2012.
26. Ceban, A., R. Pusca, and R. Romary, "Study of rotor faults in induction motors using external magnetic field analysis," *IEEE Trans. Ind. Elec.*, Vol. 59, No. 5, 2082–2093, 2012.
27. Sahraoui, M., A. Ghoggal, S. E. Zouzou, and M. E. Benbouzid, "Dynamic eccentricity in squirrel cage induction motors — Simulation and analytical study of its spectral signatures on stator currents," *Simulation Modelling Practice and Theory*, Vol. 16, No. 9, 1503–1513, Oct. 2008.
28. Dorrell, D. G., W. T. Thomson, and S. Roach, "Analysis of air gap flux, current, and vibration signals as a function of the combination of static and dynamic air gap eccentricity in 3-phase induction motors," *IEEE Trans. Ind. Appl.*, Vol. 33, 24–34, 1997.
29. Nandi, S., R. M. Bharadwaj, and H. A. Toliyat, "Performance analysis of a three-phase induction motor under mixed eccentricity condition," *IEEE Trans. Energy Conversion*, Vol. 17, No. 3, 392–399, Sep. 2002.
30. Faiz, J., I. T. Ardekanei, and H. A. Toliyat, "An evaluation of inductances of a squirrel-cage induction motor under mixed eccentric conditions," *IEEE Trans. on Energy Conversion*, Vol. 18, No. 2, Jun. 2003.